[2] Smith, T. B. and Beesmer, K. M., "Contrail Studies of Jet Aircraft," ASTIA AD 217 188, April 1959, Meteorology Research Inc., Pasadena, Calif.

[3] Scorer, R. S., *Natural Aerodynamics*, Pergamon Press, New York, 1958, pp. 73–75.

[4] Batchelor, G. K., *An Introduction to Fluid Dynamics*, Cambridge University Press, Cambridge, England, 1967, p. 509.

[5] Rosenhead, L., "The Spread of Vorticity in the Wake behind a Cylinder," *Proceedings of the Royal Society*, Ser. A, Vol. 127, 1930, pp. 590–612.

[6] Hama, F. R., "Progressive Deformation of a Curved Vortex Filament by its Own Induction," *The Physics of Fluids*, Vol. 5, No. 10, Oct. 1962, pp. 1156–1162.

[7] Thomson, Sir W., "Vibrations of a Columnar Vortex," *Mathematical and Physical Papers*, Vol. 4, Cambridge University Press, Cambridge, England, 1910, pp. 152–165.

[8] Jahnke, E. and Emde, F., *Tables of Functions*, 4th ed., Dover, New York, 1945, pp. 3–9.

[9] Watson, G. N., *Theory of Bessel Functions*, 2nd ed., Cambridge University Press, Cambridge, England, 1952, pp. 698–713.

[10] Lamb, Sir H., *Hydrodynamics*, 6th ed., Cambridge University Press, Cambridge, England, 1932, p. 241.

[11] Tung, C. and Ting, L., "Motion and Decay of a Vortex Ring," *The Physics of Fluids*, Vol. 10, No. 5, May 1967, pp. 901–910.

DECEMBER 1970 AIAA JOURNAL VOL. 8, NO. 12

# Boundary-Layer Displacement and Leading Edge Bluntness Effects on Attached and Separated Laminar Boundary Layers in a Compression Corner. Part I: Theoretical Study

MICHAEL S. HOLDEN*
*Cornell Aeronautical Laboratory, Inc., Buffalo, N.Y.*

**This paper describes a theoretical analysis of highly cooled attached and separated regions of shock wave-laminar boundary-layer interaction in the presence of strong streamwise pressure gradients generated by boundary-layer displacement effects at the leading edge. This method is an extension of an earlier analysis by Holden[1,12] to conditions where the inviscid flow cannot be described by simple isentropic flow relationships, and where the boundary-layer upstream of the main interaction is subjected to a strong pressure gradient. The analysis is compared with measurements described in Part II of the study. For strong leading edge displacement effects ($\bar{\chi}_L > 1$), the analysis predicts that highly cooled boundary layers in hypersonic flow will be supercritical; a supercritical-subcritical jump is therefore required to join the solution to the subcritical viscous layer at separation. An examination of the experimental measurements indicates that the supercritical-subcritical jump does not reflect a sudden and basic change in the flow mechanics of separation, but is an approximation necessary because the conventional boundary-layer equations cannot adequately describe the viscous interaction process leading to separation. For some high Mach number, low Reynolds number conditions, we were unable to obtain a unique solution, without recourse to experimental data, by locating a critical point in the throat region of the flow. As in the separated region, there is serious question whether the conventional boundary-layer equations can be used to adequately describe the mechanism of boundary-layer reattachment in these flows.**

## Nomenclature

$a$ = speed of sound
$C_F$ = the skin-friction coefficient
$C_H$ = the surface heat-transfer coefficient
$C_P, C_V$ = specific heats of the gas at constant pressure and at constant volume, respectively
$C$ = the constant of proportionality in the linear viscosity-temperature relation $\mu/\mu_\infty = CT/T_\infty$
$C_*$ = $[\mu(T^*)/\mu(T_\infty)]T_\infty/T_*$
$D_N$ = drag of the blunt leading edge
$h$ = static enthalpy
$h_S, H$ = total enthalpy
$k$ = leading edge drag coefficient $D_N/\frac{1}{2}\rho_\infty U_\infty{}^2 t$
$L$ = reference length
$M$ = Mach number
$p$ = pressure
$Pr$ = Prandtl number
$q$ = local surface heat-transfer rate
$Re_x$ = Reynolds number $\rho ux/\mu$
$S$ = enthalpy function $h_e/h_{S_e} - 1$
$S_W$ = $h_W/h_{S_e} - 1$
$t$ = leading edge thickness
$U, V$ = the velocity components parallel to the $x$ and $y$ axes, respectively
$x, y$ = coordinates parallel to and normal to the surface, respectively
$\gamma$ = specific heat ratio
$\delta, \delta^*$ = boundary-layer thickness and displacement thickness, respectively
$\epsilon$ = $\gamma - 1/\gamma + 1$
$\theta$ = wedge angle
$\Theta$ = local angle between $x$ axis and streamline at the edge of the boundary layer
$\kappa_\epsilon$ = a parameter controlling inviscid tip bluntness effect, $\kappa_\epsilon = M^3 kt/x$
$\mu$ = dynamic viscosity

Presented as Paper 68-68 at the AIAA 6th Aerospace Sciences Meeting, New York, January 22–24, 1968; submitted January 29, 1969; revision received April 14, 1970. This research was sponsored by the Aerospace Research Laboratories, Office of Aerospace Research, United States Air Force under Contract F33615-67-C-1298.

* Principal Aerodynamicist, Aerodynamic Research Department. Associate AIAA.

$\rho$ = gas density
$\tau$ = shear stress $\mu\partial u/\partial y|_W$
$\chi_L, \bar{\chi}_L, \chi_\theta$ = $[M^3C^{1/2}/(Re_L)^{1/2}][M^3C^{*1/2}/(Re_L)^{1/2}]\epsilon(0.664 + 1.73 T_W/T_o)\chi_L$
$\omega$ = the constant exponent in the relation $\mu\alpha T^\omega$

***Subscripts***

$e$ = local conditions in the inviscid flow just outside the boundary layer
incip = conditions relating to incipient separation
$L$ = based on the reference length
$O$ = conditions at the beginning of the corner interaction
plateau = conditions in the constant pressure region between separation and reattachment
$S$ = stagnation conditions
$\infty$ = pertaining to freestream conditions
$W$ = conditions evaluated at the wall
$*$ = based on the reference temperature $T^*$

## 1. Introduction

IN high Mach number, low Reynolds number flow, the growth of a boundary layer over a compression surface and its interaction with the external inviscid stream play an important role in determining the aerodynamic characteristics of the surface. Two important examples are the interaction between the viscous and inviscid flow on an intake compression ramp of a hypersonic air-breathing booster, and at a wing-flap junction of a control surface on a hypersonic glide vehicle. In such cases, the shock wave-boundary-layer interaction, if not correctly allowed for, can modify significantly the design performance of the surface. In many cases, the adverse pressure gradients generated by the viscous-inviscid interaction can become of sufficient strength to reverse locally the direction of the flow at the wall, thus creating a separation bubble containing recirculating flow. In the high Mach number, low Reynolds number regime, where these effects are important, attached and separated laminar boundary layers have been found to be very stable; thus, theoretical and experimental studies of shock wave-laminar boundary-layer interaction are of considerable practical importance.

The flow structure of attached and separated regions described is extremely complex, even if the viscous layer is completely laminar. In order to simplify the problem, it is possible in many cases to divide the flowfield into two regions: 1) a localized interaction region, where there is strong interaction between the inviscid flow and the nonsimilar development of the viscous layer—for example, the impingement of a shock on a boundary layer or growth of a boundary layer over a surface discontinuity, and 2) regions preceding and following this shock wave-boundary-layer interaction, where boundary-layer development can be considered locally self-similar. The term "shock wave-boundary-layer interaction" is used here to indicate the general interaction between the viscous and inviscid flow promoted by a disturbance in the inviscid stream, whether by an incident shock or by a compression corner. The structure and development of the viscous and inviscid flow from the leading edge to the beginning of the localized shock wave-boundary-layer interaction is governed by the freestream conditions, the shape of the leading edge and compression surface, and the degree of interaction between the viscous and inviscid flow. The majority of the published theoretical and experimental studies of shock wave-boundary-layer interaction on compression surfaces has considered flows in which the boundary layer immediately upstream of the interaction can be considered to be developing under constant pressure.

### 1.1 Qualitative Features of the Flow

The separated flows we will discuss are those in which the separation of the viscous layer is the result of the free interaction between a laminar boundary layer and the outer flow in the absence of surface curvature or leading edge bluntness. There are, in general, two types of configurations upon which such flows are generated: one is the impingement of a shock onto a boundary layer over a flat plate, and the second is the interaction resulting at the junction of a wedge mounted on a flat plate. Some of the basic similarities between these two types of flows are discussed in Ref. 1. Our purpose is to compare and contrast the salient features of interaction regions as generated by supersonic and by hypersonic flows past a flat plate-wedge compression surface. Figure 1 shows schematic diagrams and a schlieren photograph of the separated flow past a flat plate-wedge compression surface in supersonic and hypersonic flow. In each case, as the flow approaches the compression surface, the boundary layer thickens and interacts with the external stream, causing a compression fan. In the supersonic flow, the interaction both upstream and at the beginning of the interaction is weak, and the flow at the edge of the viscous layer is turned almost isentropically through a compression fan which coalesces to form the separation shock well downstream of this region. In contrast, in hypersonic flow, the compression in the separation region takes place more abruptly and results in the formation of a strong shock at the edge of the viscous layer which lies almost parallel with the developing boundary layer. In both supersonic and hypersonic flow, it has been found from experiment that the interaction in the separation region is followed by a region in which the separated shear layer grows under approximately constant pressure. Compression fans are again generated in the reattachment region, where the flow begins to turn parallel to the wedge. In supersonic flow, the compression fans coalesce to form a reattachment shock outside the interaction region, whereas in the hypersonic flow a strong shock is formed immediately at the edge of the boundary layer. Downstream of reattachment, the boundary layer thins to a local minimum—the neck—before relaxing to grow under approximately constant pressure downstream of the interaction.

In high Mach number, low Reynolds number flow, the strength of the interaction between the growth of the boundary layer and the inviscid stream over the basic flat plate can be of the same order as the interaction developed at the flat plate-wedge junction. The strong interaction developed close to the leading edge causes a negative pressure gradient in the inviscid flow outside the boundary layer. This favorable pressure gradient results in a fuller velocity profile in the boundary layer close to the wall relative to the corresponding Blasius constant pressure distribution, and thus has an inhibiting effect on flow separation.

### 1.2 Previous Analyses

Most of the analyses of attached and separated regions induced by shock wave-boundary-layer interaction have been based on the assumption that these regions are small and the boundary-layer equations are valid. In general, the techniques for solving separated flows are extensions of theoretical methods for solving for the development of unseparated boundary layers in a pressure gradient.

The complex nature of shock-induced separated flows and the models required to describe them have resulted almost exclusively in methods based on the solutions to the integral forms of the boundary-layer equations. The Crocco-Lees[2] method was the first of such analyses to give some measure of agreement with experiment. Rather than satisfy the momentum equation at the wall, Crocco and Lees introduced a conservation equation relating the entrainment of mass from the external inviscid flow to a mixing-rate parameter. The mixing-rate parameter can be specified either from theory,[2,3] or experiment[4]; however, the rates based on

experiment appear to give far better agreement with experimental pressure measurements. To eliminate the semi-empirical features of the latter analysis, Abbott, Holt and Nielsen[5] used a method based on an integral technique developed by Tani.[6] In adiabatic flows, the theory was in good agreement with experimental pressure measurements up to the separation point, but downstream of this point the theory did not predict the characteristic plateau found in their experiments. In highly cooled flow, their theory predicted heat transfer from the wall to the separated region, a feature not observed in experimental studies. Nielsen, Lynes and Goodwin[7] subsequently rejected this technique in favor of a multi-moment method similar in form to that developed by Dorodnitsyn.[8] They obtained good agreement between theory and experimental pressure distributions up to reattachment on flat plate-wedge compression surfaces for both adiabatic and highly cooled wall conditions. No comparisons were made between theory and measurements of heat transfer or skin friction.

Lees and Reeves[9] were the first to derive an analysis capable of successfully predicting the size and properties of shock-induced laminar separated flows over an adiabatic wall without some recourse to experiment. The theory was found to be in good agreement with measurements of pressure made in shock-induced separated regions over an adiabatic wall in Mach 2.67 and 6 airflows. However, in highly cooled flow at Mach 10, where it has been found experimentally that the heat transfer decreases, Holden[1] found that the Lees and Reeves theory predicted an increase in heating. It was suggested that in these flows, the energy dissipated in and convected across the viscous layer must be accounted for by satisfying the conservation of energy in the boundary layer. A theoretical analysis based on solutions to the integral forms of the boundary-layer equations, including the energy equation, was derived (Ref. 1). The theory was found to be in good agreement with heat transfer and pressure measurements in a Mach 10 airflow over a highly cooled wall, and with the Lees and Reeves theory and experimental measurements over an adiabatic wall in a Mach 6 airflow. This analysis is strictly valid only for flows where the interaction is weak upstream of the interaction region and where the Prandtl-Meyer theory can be used to relate the inclination of the shear-layer edge to the local Mach number. In high Mach number, low Reynolds number flows (large values of the viscous interaction parameter $\bar{\chi}_L$), the pressure gradient developed by the strong viscous-inviscid interaction over the basic flat plate, and the nonisentropic compression in the main interaction regime must be taken into account.

### 1.3 Purpose and Scope of this Study

The purpose of this paper is to extend the analysis of regions of shock wave-boundary-layer interaction described in Ref. 1 to conditions where the inviscid flow cannot be described by simple isentropic flow relationships, and where the boundary layer upstream of the main interaction is subjected to a strong pressure gradient. These conditions arise when there are strong boundary-layer displacement and leading edge bluntness effects or where the boundary layer develops over a curved surface upstream of the interaction region. In addition, we wished to explore the limitations of this integral method under high Mach number, low Reynolds conditions by a critical comparision with the detailed experimental studies described in Part II of this paper.

## 2. Present Analysis

### 2.1 Integral Forms of the Boundary-Layer Equations

In this analysis, we use the integral forms of the boundary-layer equations for the conservation of mass, momentum,

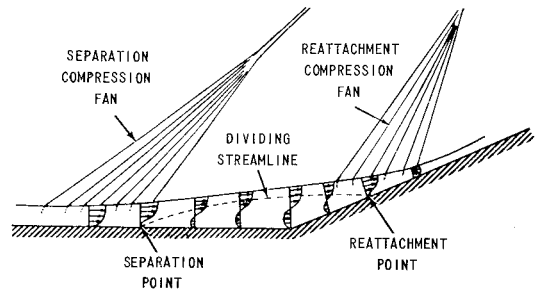


**a) supersonic separated flow**

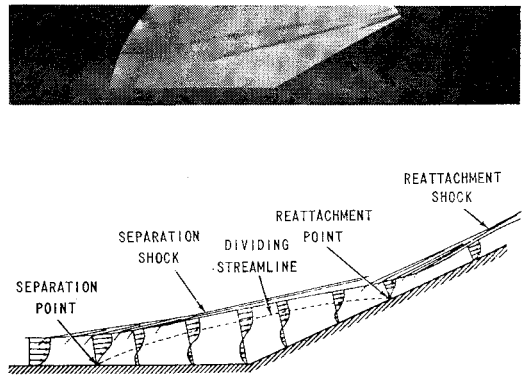


**b) hypersonic separated flow**

**Fig. 1 Supersonic and hypersonic flows.**

moment of momentum, and energy to describe the development of the boundary layer and its interaction with the outer inviscid flow. We assume that the pressure gradients normal to the edge of the boundary layer are negligible compared with the streamwise gradients. Using the Stewartson-Illingworth transformation

$$dY = \frac{a_e\rho}{a_\infty\rho_\infty}\,dy,\ dX = \frac{C}{v}\frac{a_e p_e}{a_\infty\rho_\infty}\,dx,\ \psi_y = \frac{C}{v}\frac{\rho u}{\rho_\infty},\ \psi_x = -\frac{\rho v}{\rho_\infty}$$

These equations transform into the incompressible form

$$\partial U/\partial X + \partial V/\partial Y = 0 \tag{1}$$

$$U\partial U/\partial X + V\partial U/\partial Y = U_e(dU_e/dX)(1+S) + \nu_\infty\partial^2 U/\partial Y^2 \tag{2}$$

and

$$UdS/dX + V\partial S/\partial Y = \nu_\infty\partial^2 S/\partial Y^2 \tag{3}$$

where the velocity $(U,V)$ in the incompressible plane is related to the stream function $\psi$ through the relations $U = \psi_Y$, $V = -\psi_X$.

Integrating the continuity Eq. (1) across the boundary layer, upon algebraic manipulation and simplification we obtain

$$\bar{\tau}\frac{dT}{dX} + \tilde{C}\frac{d}{dX}\log_e\delta_i^* + \frac{dH}{dX} + F\frac{d}{dX}\log_e M_e = -\frac{\nu_\infty g}{a_\infty\delta_i^{*2}M_e} \tag{4}$$

where

$$\delta_i^* = \int_0^{\delta_i}\left[1-\frac{U}{U_e}\right]dY;\ \theta_i = \int_0^{\delta_i}\left[\frac{U}{U_e}\right]\left[1-\frac{U}{U_e}\right]$$

$$I = \int_0^{\delta_i}\frac{S}{S_W}\,dY;\ K = \int_0^{\delta_i}\frac{S}{S_W}\frac{U}{U_e}\,dY$$

$$H = \frac{\theta_i}{\delta_i^*},\ T = \frac{K}{\delta_i^*},\ t = \frac{I}{\delta_i^*},\ W = \frac{1}{\delta_i^*}\int_0^{\delta_i}\frac{U}{U_e}\,dY$$

and

$$F = S_w t\left[1 - \left(\frac{1+m_e}{m_e}\right) M_e \frac{d}{dM_e}\log_e\left(\frac{p_e}{p_\infty}\right)\right] + H\left[\frac{m_e+2}{m_e+1} - M_e\frac{d}{dM_e}\log_e\frac{p_e}{p_\infty}\right] - \frac{W}{m_e}\left[\frac{2m_e+1}{m_e+1} + M_e\frac{d}{dM_e}\log_e\frac{p_e}{p_\infty}\right] + \left[1 - \left(\frac{m_e+1}{m_e}\right) M_e\frac{d}{dM_e}\log_e\left(\frac{p_e}{p_\infty}\right)\right]$$

$$m_e = \left(\frac{\gamma-1}{2}\right) M_e^2,\ M_e = \frac{u_e}{a_e} = \frac{U_e}{a_\infty},\ \tilde{\tau} = S_W\frac{m_e+1}{m_e}\frac{dt}{dT}$$

$$\tilde{C} = H + \left(\frac{m_e+1}{m_e}\right)(1+S_W t),\ g = -\frac{a_\infty M_e\delta_i^*}{\nu_\infty}\frac{1+m_e}{m_e(1+m_\infty)}\tan\Theta$$

Integrating Eq. (2) across the boundary layer and using Eq. (1), we obtain

$$H\frac{d}{dX}\ln\delta_i^* + [2H+1+S_W t]\frac{d}{dX}\ln M_e + \frac{dH}{dX} = \frac{\nu_\infty P}{a_\infty M_e(\delta_i^*)^2} \tag{5}$$

Multiplying Eq. (2) by $U$ and integrating across the boundary layer, we obtain the kinetic energy or moment of momentum equation

$$J\frac{d}{dX}\ln\delta_i^* + (3J+2S_W T)\frac{d}{dX}\ln M_e + \frac{dJ}{dH}\frac{dH}{dX} = \frac{\nu_\infty R}{a_\infty M_e(\delta_i^*)} \tag{6}$$

Integrating the energy Eq. (3) across the boundary layer, we obtain

$$T\frac{d}{dX}\ln\delta_i^* + T\frac{d}{dX}\ln M_e + \frac{dT}{dX} = -\frac{\nu_\infty Q}{a_\infty M_e(\delta_i^*)^2} \tag{7}$$

where

$$J = \frac{\theta_i^*}{\delta_i^*} = \frac{\int_0^{\delta_i}\frac{U}{U_e}\left[1-\left(\frac{U}{U_e}\right)^2\right]dY}{\int_0^{\delta_i}\left(1-\frac{U}{U_e}\right)dY};\ Q = \frac{d}{dY}\left(\frac{S}{S_W}\right)_{Y=0}\delta_i^*$$

$$P = \frac{\delta_i^*}{U_e}\left(\frac{dU}{dY}\right)_{Y=0};\ R = \frac{2\delta_i^*}{U_e^2}\int_0^{\delta_i}\left(\frac{\partial U}{\partial Y}\right)^2 dY$$

Equations (4–7) are four simultaneous, nonlinear ordinary differential equations which are functions of the displacement thickness $\delta_i^*$ the Mach number $M_e$ of the inviscid flow just outside the boundary layer, and the velocity and enthalpy profiles. Solving for these quantities, we obtain

$$\frac{\delta_i^*}{M_e}\frac{dM_e}{dX} = \frac{1}{\left(\frac{a_e M_e\delta_i^*}{\nu_\infty}\right)}\frac{M_1(T,H,M_e,g)}{c(H,T,M_e)} \tag{8}$$

$$\delta_i^*\frac{dH}{dX} = \frac{1}{\left(\frac{a_e M_e\delta_i^*}{\nu_\infty}\right)}\frac{M_2(H,T,M_e,g)}{C(H,T,M_e)} \tag{9}$$

$$\frac{d\delta_i^*}{dX} = \frac{1}{\left(\frac{a_e M_e\delta_i^*}{\nu_\infty}\right)}\frac{M_3(H,T,M_e,g)}{C(H,T,M_e)} \tag{10}$$

$$\delta_i^*\frac{dT}{dX} = \frac{1}{\left(\frac{a_e M_e\delta_i^*}{\nu_\infty}\right)}\frac{M_4(H,T,M_e,g)}{C(H,T,M_e)} \tag{11}$$

where

$$M_1 = \tilde{\tau}\left[T\left(P\frac{dJ}{dH} - R\right) + Q\left(H\frac{dJ}{dH} - J\right)\right] + \left(\frac{m_e+1}{m_e}\right)(1+S_W t)\left(R - P\frac{dJ}{dH}\right) + (P+g)\left(J - H\frac{dJ}{dH}\right)$$

$$M_2 = \tilde{\tau}\{T[R(H+1+S_W t) - P(2J+2S_W T)] + Q[J(H+1+S_W t) - H(2J+2S_W T)]\} + \left(\frac{m_e+1}{m_e}\right)(S_W t+1)[(3J+2S_W T)P - R(2H+1+S_W t)] + (P+g)[H(3J+2S_W T) - FJ] + [F-(2H+1+S_W t)][RH+Jg]$$

$$M_3 = \tilde{\tau}\left\{Q\left[(3J+2S_W T) - (2H+1+S_W t)\frac{dJ}{dH}\right] + T\left(R - P\frac{dJ}{dH}\right)\right\} + (P+g)\left[F\frac{dJ}{dH} - (3J+2S_W T)\right] - [F-(2H+1+S_W t)]\left[R + g\frac{dJ}{dH}\right]$$

$$M_4 = \left(\frac{m_e+1}{m_e}\right)(1+S_W t)\left\{\frac{dJ}{dH}[(2H+1+S_W t)Q + PT] - [TR + Q(3J+2S_W T)]\right\} + [F-(2H+1+S_W t)]\left[JQ + TR - \frac{dJ}{dH}(HQ+PT)\right] + (P+g)T\times\left[(2J+2S_W T) - \frac{dJ}{dH}(H+1+S_W t)\right]$$

$$C = \tilde{\tau}T\left[(H+1+S_W t)\frac{dJ}{dH} - (2J+2S_W T)\right] + [(2H+1+S_W t) - F]\left[J - H\frac{dJ}{dH}\right] + \left(\frac{m_e+1}{m_e}\right)\times(1+S_W t)\left[(3J+2S_W T) - (2H+S_W t+1)\frac{dJ}{dH}\right]$$

To evaluate $M_1 \ldots C$, we must specify a system of profiles to represent the form of the velocity and enthalpy distributions in both the attached and separated regions of the viscous shear layer.

### 2.2 Velocity and Enthalpy Profiles

In the conventional application of momentum integral technique, the distribution of velocity and temperature are represented by polynomials. Experience has indicated that velocity and temperature distributions represented by single-parameter polynomial profiles will not adequately describe the complex nonsimilar development of the viscous layer in both the attached and separated regions (see Ref. 1). Lees and Reeves showed that, in adiabatic flows, choosing the velocity profiles from solutions to the compressible-flow analogs of the Falkner-Skan equations gave solutions which were in good agreement with experiment. The present author (Ref. 1) has used the velocity and enthalpy profiles from the Falkner-Skan equations to obtain good agreement with heat transfer and pressure measurements in separated regions.

**Table 1 Single-parameter profiles ($S_w = -0.8$)**

| | $C_0$ | $C_1$ | $C_2$ | $C_3$ | $C_4$ |
|---|---|---|---|---|---|
| A) Attached region | | | | | |
| $J$ | +0.31913E + 00 | +0.21801E + 00 | −0.26821E − 01 | 0 | 0 |
| $H$ | +0.21511E + 00 | +0.13836E + 00 | −0.20781E − 01 | 0 | 0 |
| $W$ | +0.85225E + 00 | +0.56174E + 00 | +0.30793E − 01 | 0 | 0 |
| $R$ | +0.14661E + 01 | −0.86597E + 00 | +0.45066E + 00 | −0.77379E − 01 | −0.90562E − 03 |
| $G$ | +0.28906E + 01 | −0.14646E + 01 | +0.25974E + 00 | 0 | 0 |
| $P$ | −0.22258E − 03 | +0.53281E + 00 | −0.13683E + 00 | +0.13831E − 01 | +0.85888E − 03 |
| $[I]$ = | [3.92880 | −9.34539 | 7.56168] | | |
| $[\partial J/\partial H]$ = | [1.58 | 0] | | | |
| B) Separated region | | | | | |
| $J$ | +0.31939E + 00 | −0.21136E + 00 | −0.24067E + 00 | −0.18380E + 01 | +0.26163E + 01 |
| $H$ | +0.21366E + 00 | −0.16137E + 00 | +0.52715E − 01 | −0.22857E + 01 | +0.28536E + 01 |
| $W$ | +0.85230E + 00 | −0.52482E + 00 | −0.11703E + 01 | 0 | 0 |
| $R$ | +0.14492E + 01 | +0.21853E + 01 | −0.67996E + 01 | +0.25656E + 02 | 0 |
| $G$ | +0.29502E + 01 | +0.93472E + 00 | +0.46388E + 01 | +0.21381E + 02 | 0 |
| $P$ | +0.93132E − 08 | −0.64628E + 00 | −0.84338E + 00 | 0 | 0 |
| $[I]$ = | [7.13022 | −33.15414 | 51.81065] | | |
| $[\partial J/\partial H]$ = | [1 × (1.79240) | 2 × (−9.62757) | 3 × (79.34132) | 4 × (−299.61763) | 5 × (455.07085)] |

Here, we will again use the solutions to the compressible-flow analogs of the Falkner-Skan equations[10] to describe the distribution of velocity and enthalpy in the attached and separated viscous layer. Following Lees and Reeves, we decouple the velocity profiles from the pressure gradient parameter $\beta$ with which they are associated in the Falkner-Skan solutions, and relate them to a parameter $a(X)$, which is defined as $(dU/U_e)/(dY/\delta_i)$ for attached flow and $Y^*/\delta_i$ for separated flow, where $Y^*$ is the distance between the wall and the point of zero velocity in the separated shear layer. In contrast to the Lees-Reeves formulation, we further decouple the enthalpy profiles from the pressure gradient parameters and the velocity profiles and relate them to the parameter $b(X)$, which is defined as $-\partial/\partial\eta[S/S_W]_W$, the enthalpy gradient at the wall in both attached and separated flows.† By specifying both $a(X)$ and $b(X)$, we define a unique pair of velocity and enthalpy profiles and, also, the integral properties associated with these profiles. The integral parameters $G$, $H$, $J$, $W$, $P$, and $R$, which are velocity-dependent, were fitted as power series in $a$ by the method of least squares and expressed in the form $H = c_o + c_1a + c_2a^2 + \ldots + c_na^n$. Similarly, integral parameters which depended only upon the enthalpy profiles were fitted as power series as a function of $b$. The functions $T$, $t$, which are functions of both $a$ and $b$, we have written in the form

$$t = \left[\int_0^{\delta_i} \frac{S}{S_W}\,dY \Big/ \int_0^{\delta_i}\left(1 - \frac{U}{U_e}\right)dY\right] = \frac{I(b)}{G(a)};$$

$$T = \left[\int_0^{\delta_i} \frac{S}{S_W}\frac{U}{U_e}\,dY \Big/ \int_0^{\delta_i}\left(1 - \frac{U}{U_e}\right)dY\right] = \frac{K(a,b)}{G(a)}$$

where $K$ has been expressed as a function of both $a$ and $b$ in the form

$$K_{a=r} = c_{0r} + c_{1r}b + c_{2r}b^2 + c_{3r}b^3$$

† Klineberg (Ref. 11) later used the same representation for the enthalpy profiles in a formulation similar to the one presented here.

The numerical values for the coefficients in these power series are presented in Tables 1 and 2.

## 3. Method of Solution and Comparison with Experiment

To obtain detailed distribution of the properties throughout the separated region, it is necessary to integrate the four nonlinear, simultaneous, ordinary differential Eqs. (8–11). For ease of computation, we rewrite these equations in the form

$$\frac{\delta^2_R}{M_e}\frac{dM_e}{dX} = \frac{1}{\delta_{i_o}{}^*\tilde{R}_{\delta i_o *}}\frac{M_1(H,T,M_e,g)}{C(H,T,M_e)} \tag{12}$$

$$\delta_R{}^2\frac{da}{dX} = \frac{1}{\delta_{i_o}{}^*\tilde{R}_{\delta^* i_o}}\frac{M_2(H,T,M_e,g)}{C(H,T,M_e)}\left(\frac{dH}{da}\right)^{-1} \tag{13}$$

$$\delta_R{}^2\frac{db}{dX} = \frac{1}{\delta_{i_o}{}^*\tilde{R}_{\delta^* i_o}}\frac{M_4(H,T,M_e,g)}{C(H,T,M_e)}\left(\frac{dT}{db}\right)^{-1} \tag{14}$$

$$\delta_R\frac{d\delta_R}{dX} = \frac{1}{\delta_{i_o}{}^*\tilde{R}_{\delta^* i_o}}\frac{M_3(H,T,M_e,g)}{C(H,T,M_e)} \tag{15}$$

where

$$\frac{dT}{db} = \left[\frac{\partial K}{\partial a}\frac{1}{G} - \frac{K}{G^2}\frac{dG}{da}\right]\frac{1}{db/da} + \frac{1}{G}\left(\frac{\partial K}{\partial b}\right)$$

$$\frac{dt}{dT} = \frac{-I\dfrac{dG}{da} + G\dfrac{dI}{db}\dfrac{db}{da}}{\left[\left(G\dfrac{\partial K}{\partial a} - K\dfrac{dG}{da}\right) + G\dfrac{\partial K}{\partial b}\dfrac{db}{da}\right]}$$

and

$$\frac{db}{da} = \frac{M_4G\dfrac{dH}{da} + \dfrac{C_1I}{G}\dfrac{dG}{da} - C_2\left[\dfrac{\partial K}{\partial a} - \dfrac{K}{G}\dfrac{\partial G}{\partial a}\right]}{C_1\dfrac{dI}{db} + C_2\dfrac{\partial K}{\partial b}};\quad \delta_R = \frac{\delta_i{}^*}{\delta_{i_o}{}^*}$$

**Table 2 Two-parameter profiles ($S_w = -0.8$)**

A) Attached region ($a$ const)

| $K_\tau(a)$ | $C_{\tau,0}$ | $C_{\tau,1}$ | $C_{\tau,2}$ | $C_{\tau,3}$ |
|---|---|---|---|---|
| $a = 0$ | +0.15175471E + 01 | −0.72172180E + 01 | +0.11826745E + 02 | −0.63025606E + 01 |
| 0.10 | +0.18011203E + 01 | −0.88815174E + 01 | +0.15672985E + 02 | −0.94931138E + 01 |
| 0.20 | +0.19488165E + 01 | −0.94261444E + 01 | +0.16466635E + 02 | −0.99203131E + 01 |
| 0.30 | +0.21698984E + 01 | −0.10659802E + 02 | +0.19335803E + 02 | −0.12352766E + 02 |
| 0.40 | +0.20648935E + 01 | −0.90958258E + 01 | +0.14316718E + 02 | −0.75081331E + 01 |
| 0.50 | +0.15990186E + 01 | −0.45597938E + 01 | +0.12212479E + 01 | +0.45449936E + 01 |
| 0.60 | +0.19621929E + 01 | −0.70348662E + 01 | +0.75104608E + 01 | −0.86050099E + 00 |
| 0.70 | +0.24617465E + 01 | −0.10830794E + 02 | +0.17942552E + 02 | −0.10509071E + 02 |
| 0.80 | +0.26562766E + 01 | −0.12016264E + 02 | +0.20952415E + 02 | −0.13201778E + 02 |
| 0.90 | +0.24993300E + 01 | −0.10287924E + 02 | +0.16001762E + 02 | −0.87533766E + 01 |
| 1.00 | +0.24997877E + 01 | −0.99011868E + 01 | +0.14745981E + 02 | −0.75962584E + 01 |
| 1.10 | +0.24348323E + 01 | −0.90152416E + 01 | +0.12229457E + 02 | −0.53838662E + 01 |
| 1.20 | +0.23420011E + 01 | −0.79167962E + 01 | +0.91739380E + 01 | −0.27174472E + 01 |
| 1.30 | +0.21656435E + 01 | −0.61468370E + 01 | +0.43280488E + 01 | +0.15302640E + 01 |
| 1.40 | +0.19282681E + 01 | −0.38776961E + 01 | −0.18729788E + 01 | +0.69940294E + 01 |
| 1.50 | +0.16958692E + 01 | −0.16956462E + 01 | −0.78009611E + 01 | +0.12209048E + 02 |
| 1.60 | +0.14622544E + 01 | −0.42663687E + 00 | −0.13484303E + 02 | +0.17176542E + 02 |
| 1.70 | +0.82327990E + 00 | +0.92636200E + 00 | −0.56416790E + 01 | +0.45363630E + 01 |
| 1.80 | +0.90028040E + 00 | +0.72437760E + 00 | −0.54229480E + 01 | +0.45363730E + 01 |
| 1.90 | +0.92101980E + 00 | +0.76494100E + 00 | −0.55111810E + 01 | +0.44735320E + 01 |

$$[\partial K_\tau/\partial b]_{b=\tau} = [1 \times C_{\tau,1} \quad 2 \times C_{\tau,2} \quad 3 \times C_{\tau,3}] \times \begin{bmatrix} b^0 \\ b^1 \\ b^2 \end{bmatrix}$$

B) Separated region ($a$ const)

| $K_\tau(b)$ | $d_{\tau,0}$ | $d_{\tau,1}$ | $d_{\tau,2}$ | $d_{\tau,3}$ |
|---|---|---|---|---|
| $a = 0$ | +0.25503995E + 01 | −0.14317280E + 02 | +0.22271415E + 02 | 0 |
| 0.1 | +0.25391994E + 01 | −0.15397563E + 02 | +0.25328549E + 02 | 0 |
| 0.2 | +0.24064996E + 01 | −0.15623209E + 02 | +0.26849987E + 02 | 0 |
| 0.3 | +0.20800995E + 01 | −0.14434495E + 02 | +0.25835702E + 02 | 0 |
| 0.4 | +0.13519996E + 01 | −0.94464247E + 01 | +0.16385704E + 02 | 0 |
| 0.5 | +0.26102050E + 00 | −0.34695036E + 01 | +0.76564012E + 01 | 0 |

$$[\partial K_\tau/\partial b]_{b=\tau} = [1 + C_{\tau,1} \quad 2 \times C_{\tau,2}] \times \begin{bmatrix} b^0 \\ b^1 \end{bmatrix}$$

C) Attached region ($b$ const)

| $K_\tau(b)$ | $d_{\tau,0}$ | $d_{\tau,1}$ | $d_{\tau,2}$ | $d_{\tau,3}$ |
|---|---|---|---|---|
| $b = 0.10$ | +0.95431848E + 00 | +0.80657860E + 00 | +0.14313870E + 00 | −0.28749421E + 00 |
| 0.12 | +0.84677488E + 00 | +0.78579783E + 00 | +0.75596551E − 01 | −0.22308809E + 00 |
| 0.14 | +0.74856360E + 00 | +0.76018156E + 00 | +0.23026597E − 01 | −0.16897598E + 00 |
| 0.16 | +0.65923940E + 00 | +0.73040806E + 00 | −0.17053265E − 01 | −0.12428721E + 00 |
| 0.18 | +0.57835864E + 00 | +0.69714813E + 00 | −0.45640344E − 01 | −0.88153888E − 01 |
| 0.20 | +0.50548176E + 00 | +0.66104062E + 00 | −0.64053345E − 01 | −0.59727057E − 01 |
| 0.22 | +0.44016622E + 00 | +0.62274829E + 00 | −0.73647290E − 01 | −0.38143220E − 01 |
| 0.24 | +0.38196936E + 00 | +0.58293097E + 00 | −0.75770084E − 01 | −0.22542356E − 01 |
| 0.26 | +0.33044973E + 00 | +0.54224405E + 00 | −0.71766414E − 01 | −0.12064866E − 01 |
| 0.28 | +0.28531168E + 00 | +0.50621736E + 00 | −0.74031510E − 01 | −0.28325382E − 03 |
| 0.30 | +0.24610467E + 00 | +0.45806257E + 00 | −0.47896495E − 01 | −0.39648282E − 02 |
| 0.32 | +0.21205355E + 00 | +0.41788290E + 00 | −0.31589646E − 01 | −0.51593696E − 02 |
| 0.34 | +0.18181475E + 00 | +0.38531394E + 00 | −0.20497446E − 01 | −0.55090511E − 02 |
| 0.36 | +0.15800381E + 00 | +0.34403285E + 00 | +0.13698642E − 02 | −0.10019273E − 01 |
| 0.38 | +0.13553251E + 00 | +0.32646906E + 00 | −0.13445932E − 01 | +0.62562437E − 03 |
| 0.40 | +0.11983134E + 00 | +0.28201795E + 00 | +0.25718330E − 01 | −0.14042450E − 01 |
| 0.42 | +0.10603855E + 00 | +0.26037654E + 00 | +0.27673312E − 01 | −0.13463867E − 01 |
| 0.44 | +0.93757623E − 01 | +0.25013257E + 00 | +0.11933836E − 01 | −0.52306838E − 02 |
| 0.46 | +0.84134592E − 01 | +0.24197740E + 00 | −0.61460123E − 02 | +0.58837109E − 02 |
| 0.48 | +0.77832328E − 01 | +0.22651030E + 00 | −0.10035929E − 01 | +0.11568039E − 01 |

$$[\partial K_\tau/\partial a]_{a=\tau} = [1 \times d_{\tau,1} \quad 2 \times d_{\tau,2} \quad 3 \times d_{\tau,3}] \times \begin{bmatrix} a^0 \\ a^1 \\ a^2 \end{bmatrix}$$

D) Separated region ($b$ const)

| $K_\tau(b)$ | $d_{\tau,0}$ | $d_{\tau,1}$ | $d_{\tau,2}$ | $d_{\tau,3}$ |
|---|---|---|---|---|
| $b = 0.05$ | +0.18855079E + 01 | +0.10346549E + 01 | −0.92150345E + 01 | 0 |
| 0.10 | +0.13599900E + 01 | −0.11670050E + 00 | −0.51859716E + 01 | 0 |
| 0.15 | +0.90500000E + 00 | −0.60196132E + 00 | −0.25374424E + 01 | 0 |
| 0.20 | +0.57999990E + 00 | −0.88995103E + 00 | −0.10323631E + 01 | 0 |
| 0.25 | +0.36000000E + 00 | −0.72195912E + 00 | −0.53396865E + 00 | 0 |
| 0.30 | +0.25800000E + 00 | −0.57601205E + 00 | −0.25203886E + 00 | 0 |

$$[\partial K_\tau/\partial a]_{a=\tau} = [1 \times d_{\tau,1} \quad 2 \times d_{\tau,2}] \times \begin{bmatrix} a^0 \\ a^1 \end{bmatrix}$$

where

$$C_1 = S_W\left(\frac{m_e+1}{m_e}\right)\{T[(RH+1+S_Wt)-P(2J+2S_WT)]+Q[J(H+1+S_Wt)-H(2J+2S_WT)]\}$$

$$C_2 = \left(\frac{m_e+1}{m_e}\right)(1+S_Wt)[(3J+2S_WT)P-R(2H+1+S_Wt)]+(P+g)[H(3J+2S_WT)-FJ]+[F-(2H+1+S_Wt)][RH+Jg]$$

Equations (12–15) are solved simultaneously to yield the variation of the basic parameters $a$, $b$, $M_e$ and $\delta_R$. To obtain a complete solution to these equations, we prescribe the freestream Mach number upstream and downstream of the interaction, together with the unit Reynolds number of the freestream. The equations are integrated numerically, using the Adams-Moulton predictor-corrector method with the Runge-Kutta method for initializing the integration. The integration is initialized upstream of the flat plate-wedge junction and proceeds through separation to the point of maximum displacement thickness at a trail distance $L_{SEP}$ downstream. From this point the equations are integrated through the reattachment point and neck region (or throat if the boundary layer is initially supercritical) to the end of the corner interaction where $dM_e/dX$, $da/dX$ and $db/dX$ return to 0. At this point the Mach number is compared with the reference value ($M_{REF}$) which has been determined from inviscid flow considerations. The trial solution is iterated by changing $L_{SEP}$ until an $a \rightarrow a_{BLASIUS}$ as $M \rightarrow M_{REF}$ when a unique solution is obtained.

### 3.1 Weak Interaction Regime

In this regime ($\bar{\chi}_L > 1$), the velocity and enthalpy profiles up and downstream of the corner interaction are assumed self-preserving and the Mach number gradient in the inviscid flow is small; hence $da/dX = db/dX = dM_e/dX = 0$. Thus, the boundary-layer equations yield the Blasius solution for the velocity and enthalpy distribution in the boundary layer as boundary conditions upstream and downstream of the corner interaction region. For small laminar separated regions in this regime the experiments have indicated that the compression wave generated by the curvature of the viscous layer does not coalesce to form strong shocks immediately above the viscous layer; thus isentropic flow relationships and, in particular, the Prandtl-Meyer expression can be used to relate the local flow inclination at the edge of the viscous layer to the local Mach number.

A comparison between experimental measurements and distributions of pressure and heat transfer calculated from Eqs. (12–15) are shown in Fig. 2. The pressure distribution is in good agreement with experiment. We note that the pressure rise to separation is approximately half the pressure rise to the plateau, and reattachment occurs at a pressure less than halfway up the reattachment pressure rise. Although the calculated heat-transfer distribution agrees well with experiment in the attached flow, theory underestimates the decrease in heat transfer to the separated region. Further comparisons between theory and experiment are contained in Refs. 1 and 12. The theory has also predicted, with good accuracy, the incipient separation[12] condition in these highly cooled flows at Mach 10 and the characteristic changes in the form of the heat transfer and pressure distributions in attached and separated flow. Solutions for the distribution of pressure in a shock-induced separated region in a Mach 6 airflow over an adiabatic wall were found to be in excellent agreement with the experimental data of Chapman, Kuehn and Larson[13] and with the theory of Lees and Reeves.[9]

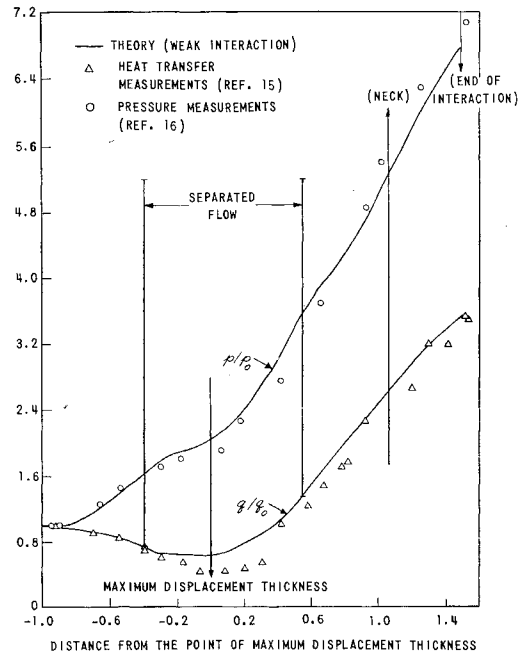


**Fig. 2 Pressure and heat transfer distributions in a highly cooled shock-induced separated flow ($S_w = -0.8$, $M_\infty = 10$, $Re_x = 1.35 \times 10^5$/in., wedge angle = 10.4°).**

### 3.2 Strong Interaction Regime

In the strong interaction regime ($\bar{\chi}_L > 5$), the interaction between the viscous and inviscid flows over the basic flat plate significantly influences the growth of the boundary layer and the distribution of velocity and enthalpy within it. Schlieren and pressure measurements taken in the experimental studies (see Part II) indicate that the inviscid flow in the corner interaction region cannot be represented by a simple wave system. In the theoretical model, on the basis of the measurements in the experimental program, we have used the tangent-wedge relationships to relate the inclination of the viscous layer to conditions in the inviscid stream. Upstream of the point of maximum displacement thickness we assumed a shock compression from freestream conditions to the local conditions at the edge of the viscous layer. Downstream of the point of maximum displacement thickness we assumed a shock compression from the conditions at the point of maximum displacement thickness to the local inclination of the viscous layer.

We have generalized the upstream boundary conditions by assuming that the velocity in the incompressible plane is given by $U_e = \bar{C}X^m$, and the pressure distribution up to the beginning of the interaction is of the form $p/p_\infty \propto x^n$. Then, for hypersonic flow, it can be shown that

$$\beta = 2\bar{m}/\bar{m} + 1 = (1-\gamma/\gamma)(n/n+1)$$

We also assume that, upstream of the main interaction, the velocity and enthalpy profiles are self-preserving, hence $da/dX = db/dX = 0$.

Solving the continuity and momentum equations, we obtain

$$\left(\frac{2}{m+1}\right)\frac{X}{M_e}\frac{dM_e}{dX} = \frac{R_FH_F - P_FJ_F}{G_F^2[H_F(J_F+2S_WT_F)-J_F]} = \frac{1-\gamma}{\gamma}\frac{n}{n+1} \quad (16)$$

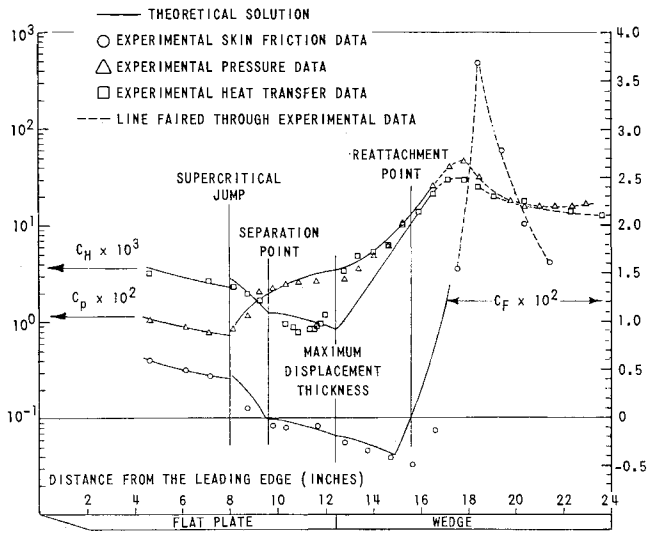


**Fig. 3 Comparison between theory and experimental measurements of skin friction, pressure and heat transfer on the sharp flat plate-wedge model ($M_\infty = 19.8$, $\bar{X}_L = 19.8$, $\theta = 25.67°$).**

and also

$$g = \left[\frac{G_F{}^2\beta}{P_F J_F - R_F H_F}\right]\left[\left(\frac{1+m_e}{m_e}\right) + H_F\right] \times [(3J_F + 2S_W T_F)P_F - R_F(2H_F + 1)] - F\beta G_F{}^2 = -\tilde{R}_{e\delta^*{}_t}\frac{(1+m_e)}{m_e(1+m_\infty)}\tan\Theta \quad (17)$$

Thus, for a given form for the pressure distribution, Eq. (16) can be solved to yield $a$ and $b$ and Eq. (17) solved for $M_e$. These values are then used to initialize the integration of the boundary-layer equations. From the present experimental pressure measurements for a strong interaction over the flat plate we find $n = 0.5$.

For the initial condition imposed by a strong favorable pressure induced by boundary-layer displacement effects at the leading edge we were unable to perform a continuous integration from the beginning of the interaction to the separation point. The initial response of the boundary layer is such that it will not support a self-induced positive pressure gradient which will lead to separation by free-interaction, i.e., the boundary layer has a supercritical response. The concept of subcritical and supercritical boundary layers was first introduced by Crocco and Lees[2] and Crocco[3] to describe the gross reaction of a viscous boundary layer when subjected to a pressure gradient within the framework of conventional boundary-layer theory. The boundary layer exhibits a supercritical response when $d\delta/dp$ is negative, and a subcritical response when $d\delta/dp$ is positive. Thus, when subjected to an adverse pressure gradient, the boundary layer with a subcritical response will thicken, whereas the supercritical boundary layer will thin. For a simple explanation of this phenomenon we consider the boundary to be composed of a supersonic and subsonic layer. The boundary layer, subjected to an adverse pressure gradient acting uniformly across its width, will thin if the contraction of the streamlines in the supersonic portion of the boundary layer is larger than the increase in the height of the subsonic layer and is termed supercritical. If the subsonic layer grows faster than the supersonic layer, the boundary layer exhibits a subcritical behavior. Thus, we can see that a subcritical boundary layer can, by interacting with the inviscid stream, develop its own positive pressure gradient, whereas no such mechanism exists if the boundary layer is supercritical. This feature is of fundamental importance when we consider the phenomenon of boundary-layer separation, since at the separation point the boundary layer is subcritical regardless of the magnitude of Mach number or the degree of wall cooling. Thus, in order to reach the separation point, the structure of the boundary layer must adjust to become subcritical.

Within the present theoretical framework the only way the supercritical boundary layer can reach separation is to adjust rapidly to give a subcritical response. The supercritical-subcritical jump has been proposed as a mechanism to join the supercritical and subcritical branches of the solution in a number of studies. Despite its appeal from the mathematical viewpoint, there is no experimental evidence to support such a discrete and abrupt transition as part of the mechanism of boundary-layer separation in hypersonic flow. The supercritical-subcritical jump should be regarded as an approximation which is necessary because of the limitation of the mathematical description in terms of the conventional boundary-layer equations rather than a natural phenomenon. Thus, here we have chosen to formulate the jump conditions in a manner to minimize the size of the discontinuity.

We assume the jump to be a shock compression from the initial supercritical conditions to conditions where the boundary layer just begins to exhibit a subcritical response. To determine the strength of the supercritical-subcritical jump we assume the process takes place over a short length so that the contributions from mass entrainment, skin friction, and surface heat transfer are negligible. The conservation equations for mass, momentum and energy then become

$$\delta_{i_1}{}^* M_{e_1} W_1 = \delta_{i_2}{}^* M_{e_2} W_2$$

$$\left(\frac{P_2}{P_1} - 1\right)\frac{P_1}{P_\infty} = \frac{2\gamma M_1 \bar{W}_1}{1 + (\bar{W}_1 M_1/\bar{W}_2 M_2)} \times \left[\frac{M_e(1+m_\infty)^{1/2}}{(1+m_e)^{1/2}}\left(1 - \frac{H}{\bar{W}}\right)\right]_2^1$$

and

$$K_1 G_2 W_2 = K_2 G_1 W_1$$

$$\bar{W} = W \Big/ \left(\frac{a_\infty \rho_\infty}{a_e \rho_e}\right)[(1+m_e)(S_W t + 1) + m_e H + W]$$

The conditions across the discontinuity in the inviscid flow, $M_e$, $a_e$, etc., are related by the oblique shock relationships. The boundary layer downstream of the jump must

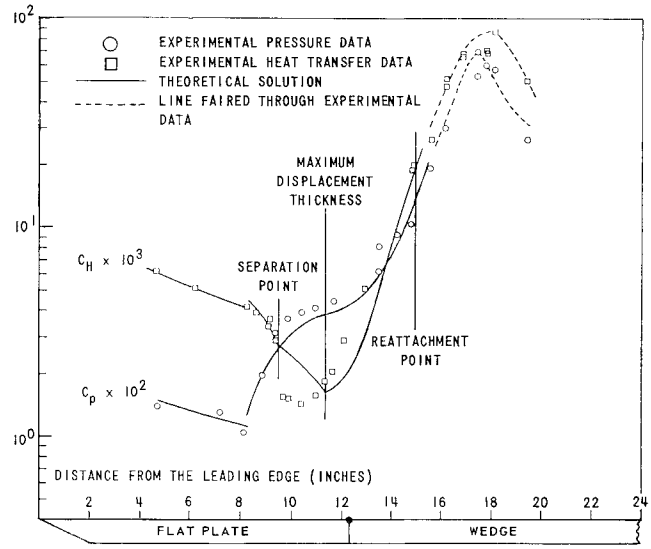


**Fig. 4 The distribution of heat transfer and pressure on the flat plate-wedge model ($M_\infty = 16$, $\bar{X}_L = 19.8$, $\theta = 31°$).**

exhibit a subcritical response, i.e., $C$ must be negative and small. Using the above equations and conditions, we can obtain the change in Mach number, displacement thickness and profile parameter across the discontinuity. Downstream of the jump, the equation can be integrated in a straightforward manner through to the throat region of the flow downstream of reattachment. A unique solution is obtained when the integration proceeds smoothly through the critical point in the throat region to asymptote to a self similar solution downstream of the corner.

The theory described above has been applied to calculate the distribution of pressure, heat transfer and skin friction in separated regions for two of the conditions examined in the experimental studies in Part II of this paper. In both of the cases chosen for comparison we were unable to integrate smoothly through the critical point in the throat region and thus obtain a unique solution without reference to experimental data. For the comparisons between theory and experiment shown in Figs. 3 and 4, the length from the beginning of the interaction to the beginning of the reattachment pressure rise was prescribed from experiment. There is generally good agreement between theory and experimental data. The heat transfer measurements exhibit a more rapid decay to reach a lower minimum than predicted by theory; these measurements indicate that the point of minimum heat transfer occurs upstream of the beginning of the reattachment compression process, whereas theory predicts these points are coincident. The present method, based as it is on solutions to the integral forms of the boundary-layer equations, will inherently describe the growth of the boundary layer and the pressure distribution more accurately than quantities such as skin friction or heat transfer, which are sensitive to the detailed form of the velocity and enthalpy profiles. The virtue of the Falkner-Skan family of velocity profiles lies in the fact that they embrace the exact constant pressure solutions of Blasius and Chapman for flat plate boundary layers and laminar free-mixing, respectively, and are similar in form and development to measurements made in regions of shock wave-boundary-layer interaction.[14] Although the enthalpy profiles derived from solutions to the Falkner-Skan equations exhibit these same bounding constant pressure solutions for attached and separated flow, there is need for experimental verification in shock-induced separated flows. An encouraging feature is that the theory predicts correctly[1] the characteristic changes in the form of the heat transfer distribution to the wall as the strength of the interaction is changed, causing the boundary layer to change from attached to separated.[15,16]

In the two solutions previously discussed, and in some cases where the boundary layer was initially subcritical but with large deflection angles, we were unable to integrate to the end of the interaction and completely satisfy the downstream boundary conditions to obtain a unique solution. In cases with initially supercritical boundary layers, we could not find solutions which passed smoothly through the saddle point singularity in the throat region. It is interesting to note that Golik, Webb and Lees[17] and Ai[18] also failed to obtain unique solutions for laminar near-wake flows under high Mach number, low Reynolds number conditions. In our experiments at Mach 16 and 20, wedge angles of up to 31° were required to promote even a small separated region, and in these flows most of the deflection of the viscous layer occurred in the reattachment region. Under these conditions the normal pressure gradients developed in the reattachment region doubtless make a significant contribution to the flow mechanics of reattachment. It is believed, therefore, that the breakdown in the present solution downstream of reattachment may result from neglecting the contribution from normal pressure gradient to the momentum balance in the reattachment region. The need for a super-subcritical jump upstream of separation may also result from a model inadequate in this respect. The development of strong pressure gradients normal to the body surface in the separation region may be a fundamental factor in determining the response of a boundary layer in high speed, low Reynolds number flows to a self-induced adverse pressure gradient. The largest pressures will occur at the bottom of the boundary layer contributing to an increased thickening of this region, thus creating a more subcritical response.‡

## Concluding Remarks

Solutions have been obtained to the integral forms of the boundary-layer equations which describe attached and separated regions of shock wave-boundary-layer interaction on highly cooled compression surfaces. The analysis is in good agreement with measurements of heat transfer and pressure in attached and separated interactions in a Mach 10 airflow. The theory has been applied to describe interactions for conditions where the boundary layer develops in a strong pressure gradient resulting from boundary-layer displacement effects at the leading edge (i.e., $\bar{\chi}_L > 5$). Under these conditions the compression process in the viscous interaction is nonisentropic and cannot be described by the simple Prandlt-Meyer relationship. In these flows the analysis indicated that the initial boundary layer is supercritical and thus will not generate a self-induced adverse pressure gradient leading to boundary-layer separation by free-interaction. Within the framework of the conventional boundary-layer equations a supercritical-subcritical jump must be postulated to join the supercritical boundary layer at the beginning of the interaction to the subcritical boundary layer at separation. An examination of the experimental measurements indicates that the supercritical-subcritical jump does not reflect a sudden and basic change in the flow mechanics of separation but is an approximation necessary because in Mach number, low Reynolds number flows over the cooled surface, the conventional boundary-layer equations cannot adequately describe the viscous interaction process leading to separation. Although we were able to successfully formulate jump conditions and integrate the equations through separation to downstream of reattachment, we were unable to locate a critical point in the throat region of the flow. In high Mach number, low Reynolds number flows there is serious question whether the conventional boundary-layer equations are capable of describing accurately the mechanism of boundary-layer reattachment. For these flows we specified strength of the interaction by specifying the distance from the beginning of the interaction to the beginning of the reattachment pressure rise from experiment. The analysis was in good agreement with the pressure, heat transfer and skin-friction measurements obtained in the experimental study described in Part II of the paper.

## References

[1] Holden, M. S., "An Analytical Study of Separated Flows Induced by Shock Wave-Boundary Layer Interaction," Rept. AI-1972-A-3 Dec. 1965, Cornell Aeronautical Lab.

[2] Crocco, L. and Lees, L., "A Mixing Theory for the Interaction Between Dissipative Flows and Nearly Isentropic Streams," *Journal of Aeronautical Sciences*, Vol. 19, No. 10, Oct. 1952, pp. 649–676.

[3] Crocco, L., "Considerations on the Shock-Boundary Layer Interaction," *Proceedings of the Conference on High-Speed Aeronautics*, Polytechnic Institute of Brooklyn, 1955, pp. 75–112.

‡ A theoretical and experimental study[19] of the effects of normal pressure gradients has been published by the author during the review of this paper which verifies the major conclusions reached here.

[4] Glick, H. S., "Modified Crocco-Lees Mixing Theory for Supersonic Separated and Reattaching Flows," *Journal of Aerospace Sciences*, Vol. 29, No. 10, Oct. 1962, pp. 1238–1244.

[5] Abbott, D. E., Holt, M., and Nielsen, J. N., "Investigation of Hypersonic Flow Separation and its Effect on Aerodynamic Control Characteristics," VIDYA Rept. 81, Sept. 1962.

[6] Tani, I., "On the Approximate Solution of the Laminar Boundary Layer Equations," *Journal of Aeronautical Sciences*, Vol. 21, No. 7, July 1954, pp. 487–504.

[7] Nielsen, J. N., Lynes, L. L., and Goodwin, F. K., "Theory of Laminar Separated Flows on Flared Surfaces Including Supersonic Flow with Heating and Cooling," *Proceedings of AGARD Fluid Dynamics Panel*, No. 6, Part I, 1966.

[8] Dorodnitsyn, A. A., "General Method of Integral Relations and its Application to Boundary Layer Theory," *Advances in Aeronautical Sciences*, edited by Von Kármán, Vol. 3, 1962.

[9] Lees, L. and Reeves, B. L., "Supersonic Separated and Reattaching Laminar Flows: I. General Theory and Application to Adiabatic Boundary Layer-Shock Wave Interactions," Tech. Rept. 3, Oct. 1963, Graduate Aeronautical Labs., California Institute of Technology.

[10] Cohen, C. B. and Reshotko, E., "Similar Solutions for the Compressible Laminar Boundary Layer with Heat Transfer and Pressure Gradient," Rept. 1293, 1956, NACA.

[11] Klineberg, J. and Lees, L., "Theory of Laminar Viscous-Inviscid Interactions in Supersonic Flow, "AIAA Paper 69-7, New York, 1969.

[12] Holden, M. S., "Theoretical and Experimental Studies of Separated Flows Induced by Shock Wave-Boundary Layer Interaction," *Proceedings from AGARD Specialists Meeting on Separated Flows*, No. 4, Part I, 1966.

[13] Chapman, D. R., Kuehn, D. M., and Larson, H. K., "The Investigation of Separated Flows in Supersonic and Subsonic Streams with Emphasis on the Effect of Transition," Rept. 1356, 1968, NACA.

[14] Hakkinen, R. J. et al., "The Interaction of an Oblique Shock Wave with a Laminar Boundary Layer," Memo 2-18-59W, March, 1959, NASA.

[15] Holden, M. S., "Experimental Studies of Separated Flows at Hypersonic Speeds. Part II, Two-Dimensional Wedge Separated Flow Studies," *AIAA Journal*, Vol. 4, No. 5, May 1966, pp. 790–799.

[16] Needham, D. A., "Laminar Separation in Hypersonic Flow," Ph.D. thesis Aug. 1965, Univ. of London, London, England.

[17] Golik, R. J., Webb, W. H., and Lees, L., "Further Results of Viscous Interaction Theory for the Laminar Supersonic Near Wake," AIAA Paper 67-61, New York, 1967.

[18] Ai, D., "On the Hypersonic Laminar Near Wake Critical Point of the Crocco-Lees Mixing Theory," AIAA Paper 67-60, New York, 1967.

[19] Holden, M. S., "Theoretical and Experimental Studies of the Shock Wave-Boundary Layer Interaction on Curved Compression Surfaces," *Proceedings of the Symposium on Viscous Interaction Phenomena in Supersonic and Hypersonic Flow*, May 1969, Univ. of Dayton Press.